J Therm Spray Tech (2021) 30:886–897
https://doi.org/10.1007/s11666-021-01154-6

PEER REVIEWED

Development of Novel Thermal Sprayed Hydroxyapatite-Rare Earth (HA-Re) Coatings for Potential Antimicrobial Applications in Orthopedics

Chunling Yang[1,2] · Jin Liu[3] · Qianhong Ren[1,2] · Yi Liu[1,2,3] · Ping Zhou[1,2] · Hua Li[1,2]

Submitted: 30 September 2020 / in revised form: 12 December 2020 / Accepted: 29 December 2020 / Published online: 20 January 2021

Abstract Biofilm-associated infections and the lack of successful tissue integration of biomaterial surfaces are the two main barriers to the long-term service of implanted biomaterials. Development of novel biocompatible antimicrobial materials has provided insights into their potential biomedical applications. Many clinical studies have successfully proved that hydroxyapatite coating has excellent osteogenic activity but lacks antibacterial infection in the early stages after implantation. Rare earth (Re) elements have become promising antibacterial biocides and bone-forming effects. Antibacterial capacity of 14 rare earth elements (Eu, Gd, Ce, Nd, Y, La, Pr, Er, Sm, Ho, Tb, Yb, Lu, Dy) was assayed. The gadolinium (Gd) showed outstanding broad-spectrum antibacterial activity against both Gram-positive and Gram-positive bacteria. Here, we report Gd-HA coatings deposited on titanium (Ti) substrate by liquid thermal spraying. The grain size of Gd-HA decreased slightly after Gd^{3+} incorporation. The antibacterial properties of Gd-HA composite coatings were determined against Gram-negative pathogens *Escherichia coli* and Gram-positive pathogens *Staphylococcus epidermidis*. The anti-infection performances were assessed by examining bacteria adhesion and biofilm formation on the coatings. The in vitro cytotoxicity of the Gd-doped HA coatings was further measured on human osteoblast cell line by CCK-8 method. The thermal sprayed HA-Re composite coatings show improved antimicrobial and biocompatible properties and great applicable potential in orthopedics.

Keywords antibacterial · biological activity · gadolinium · HA-Re coating · rare earth · thermal spraying

This article is an invited paper selected from presentations at the 10th Asian Thermal Spray Conference (ATSC 2020) and has been expanded from the original presentation. ATSC 2020 was held in Ningbo, China, from November 1-3, 2020, and was organized by the Asian Thermal Spray Society with Ningbo Institute of Materials Technology and Engineering, Chinese Academy of Sciences as the Host Organizer.

✉ Yi Liu
liuyi@nimte.ac.cn

[1] Key Laboratory of Marine Materials and Related Technologies, Zhejiang Key Laboratory of Marine Materials and Protective Technologies, Ningbo Institute of Materials Technology and Engineering, Chinese Academy of Sciences, Ningbo 315201, China

[2] Zhejiang Engineering Research Center for Biomedical Materials, Cixi Institute of Biomedical Engineering, Ningbo Institute of Materials Technology and Engineering, Chinese Academy of Sciences, Ningbo 315201, China

[3] Institute of Applied Physics, Jiangxi Academy of Sciences, Nanchang 330029, China

Introduction

Due to dramatical growth of the global elderly population and orthopedic device market (Ref 1, 2), the implanted biomaterials have become one of the most clinically demanded medical materials (Ref 2). The development of bone tissue engineering relies on the development of alternative materials for implanted biomaterials (Ref 3). The ideal implanted materials should possess good biocompatibility, low cytotoxicity, inducibility, regeneration, and mechanical wear resistance (Ref 4). Hydroxyapatite (HA) is a biologically active ceramic material, possessing good biocompatibility, high osteo-conductivity, and osteoinduction (Ref 5). It improves the formation of chemical bonds between artificial implants and host bone and easily adsorbed by osteoblasts to promote the growth

of osteoblasts owing to its chemical similarity to the bone mineral components (Ref 6, 7). Therefore, it has been widely applied in the biological field (Ref 8). Biomaterials incorporated in the human body should possess antibacterial properties as they are exposed to bacterial colonization. Bacteria can easily develop a biofilm structure on implants and protect themselves from environment conditions and human immune system, making the implant invalid and even threatening the life of the patient (Ref 9), which requires the implant material have long-lasting antibacterial properties (Ref 10). Whereas, pure hydroxyapatite itself does not possess antibacterial properties. Consequently, many authors have conducted antibacterial modification studies on hydroxyapatite, hoping to endow HA with antibacterial property (Ref 11).

Based on the study of the crystal structure of HA, doping antibacterial elements in hydroxyapatite is a common method for antibacterial modification (Ref 12), in which a variety of metal ions can replace calcium ions. As reported, many antibacterial ions have been used to modify HA to make it antibacterial, such as Ag^{+}, Cu^{2+}, Mg^{2+}, Ce^{3+}/Ce^{4+}, Y^{3+} etc. (Ref 13). Among them, Ag^{+} and Cu^{2+} are most studied which are antibacterial elements that discovered and applied earlier with broad-spectrum and excellent antibacterial properties, Recent studies suggested that their doping attribute to HA good antibacterial properties, but because of the poor biological properties and certain cytotoxicity of Ag^{+} and Cu^{2+}, their application were limited (Ref 14, 15). To avoid these drawbacks, new elements are to be explored.

Rare earth elements (Re) possess quite strong broad-spectrum antibacterial properties in the ionic state, so the doping of rare earth element ions to modify HA is a research hotspot (Ref 16). Re refers to 15 elements in the lanthanides, as well as two elements related to the lanthanides scandium (Sc) and yttrium (Y). The peculiarity of their electron shells structure makes them unique physiological and biochemical characteristics (Ref 17). They show positive effects on anti-inflammatory, antibacterial, anti-cancer and anti-tumor (Ref 18). Moreover, studies have found that trace amounts of rare earth elements (La, Ce, Gd, Yb, etc.) were contained in the inorganic salt components of human hard tissues, which play an important role in regulating the functions of cells or tissues (Ref 19, 20). Based on the above characteristics, doping a certain amount of rare earth elements into hydroxyapatite as a bone repair materials can not only improve the antibacterial properties of the material, but also ensure its good biocompatibility (Ref 21). Recently, various rare earth elements and their compounds have been studied for biomedical field.

Gadolinium (Gd) is a rare earth element belonging to the lanthanide series, which has been employed in microwave technology and energy industry (Ref 22, 23). The current research indicates the Gd possesses antimicrobial performance, especially well synergistic antibacterial properties, low cytotoxicity, and well biocompatibility, has been applied in tumor treatment, drug delivery, and biomedical imaging (MRI, x-raying imaging) (Ref 24, 25). Gd-containing magnesium alloys and Gd-doped scaffolds as orthopedic implants exhibited no cytotoxicity to L929, MG63, VSMC cells and animal test. Furthermore, the addition of Gd element effectively activated the Wnt/β-catenin signaling pathway and subsequently improve bone marrow mesenchymal stem cell proliferation and osteogenic differentiation (Ref 26, 27). Gd ion is exist in the form of Gd^{3+} (0.0938 nm) is similar to Ca^{2+} (0.1000 nm) in ionic radius and characters, it possesses higher charge and a larger ion potential compare to Ca^{2+}. Furthermore, the binding stability of Gd^{3+} is higher than Ca^{2+} for compounds bound by ionic bonds, makes it feasible to replace Ca^{2+} into the crystal lattice of HA (Ref 13). Besides, according to the Born-Lande formula (Ref 28): $U = KZ_1Z_2A(1 - 1/n)/r$, where A is the Madelung constant, K is 138,940, $|Z_1|$ is the Cation charge, $|Z_2|$ is the Anion charge, r is the nucleus distance, n is the Born index. The incorporation of Gd^{3+} increases the lattice energy of HA and improves its crystal stability. In these regards, incorporating Gd^{3+} into HA is an appropriate method to make it a promising biomaterial possesses good biocompatibility, antibacterial performance, and good stability.

The coating technology has been recognized as a commercial method to improve the functional performance and service life of artificial implants for tissue engineering (Ref 29, 30). Specifically, thermal spraying is a industrialized coating process whereby heat sources (flame, plasma, electric arc, etc.) are used to adjust the molten state of feedstocks that are accelerated in a fluid stream (Ref 31). Thermal spray coatings from powders require it suitable particle size range and good fluidity that need a series of cumbersome processes to be achieved (Ref 32). The use of suspension feedstock is one of the most recent and promising innovations in the thermal technology (Ref 33), due to it no need for secondary granulation, controlling grain growth, simplify the process, high deposition efficiency and the prepared coatings are nanostructure (Ref 34), most remarkably, suspension spraying gives the possibility to deposit thin (< 20 μm) and dense layers for surface modification of medical devices (Ref 35).

At the present work, the antibacterial effects of 14 rare earth elements on Gram-positive bacteria and Gram-negative bacteria were initially screened. Then, Gd^{3+} doped HA into precursors were synthesized by liquid precipitation method (Ref 36) and their composite coatings on titanium were further prepared by liquid thermal spraying (Ref 37). The antibacterial properties of as-sprayed coating were

investigated against the typical bacterial strains *Escherichia coli* and *Staphylococcus epidermidis*. The adhesion and colonization phenomena of bacteria were observed. The results demonstrate that a bio-coating material with excellent antibacterial properties and promoted bone growth was prepared, which show potential for the antimicrobial applications in tissue engineering.

Materials and Methods

Commercially available rare oxide powders (YumYi Rare Earth Inc., Ganzhou, China) were used for biocides. Nano-HA, Gd_x-HA powder was synthesized by thermal precipitation method (Ref 38) utilizing $Gd(NO_3)_3{\cdot}6H_2O$ (Jiangxi Academy of Sciences, China), $Ca(NO_3)_2{\cdot}4H_2O$ (Aladdin, China) and $(NH_4)_2HPO_4$ (Aladdin, China). The ammonia water ($NH_3{\cdot}H_2O$, Sinopharm Group Co., Ltd., China) was used for PH regulation. According to the theoretical calculation of molar ratio, HA slurry, 5 mol.% Gd-HA, 7.5 mol.% Gd-HA, and 10 mol.% Gd-HA slurries were prepared. Titanium alloy with 15 × 15 mm^2 in length and width as well as 2 mm in thickness was used as the substrates. Prior to coating deposition, the substrates were mechanically roughened via sand blasting and ultrasonically cleaned in acetone. The coatings were subsequently produced by liquid flame spraying. The Gd-HA composite slurry was atomized and injected into the flame source with liquid feed rate of 80 $mL{\cdot}min^{-1}$ and a nitrogen flow rate of 0.01 $L{\cdot}min^{-1}$. Preparation process of feedstock and subsequent coating has been schematically depicted (Fig. 1). The spray parameters were conducted at a spray distance of 150 mm, an oxygen flow rate of 42.9 $L{\cdot}min^{-1}$, and a propane flow rate of 7.34 $L{\cdot}min^{-1}$.

The phase composition of the powders and coatings was evaluated by x-ray diffraction (XRD) with German Bruker AXS D8 Advance diffractometer using Cu Kα1 radiation (λ = 1.54060 Å). Scanning electron microscopy with energy-dispersive x-ray spectroscopy (SEM–EDX, Quanta FEG 250, FEI, Oxford, Ohio, USA) was used to analyze the surface morphology, elemental distributed of the powders and coatings. The surface morphology and roughness Ra of as-sprayed coatings were measured via laser confocal microscope (3D optical Proficometer, UP-Lambda 2, Rtec Instruments, San Jose, USA). The lattice structure of $Gd_{0.1}$-HA powders was investigated through high-resolution transmission electron microscope (HRTEM, Tecnai F20, USA).

Gram-positive bacteria *Staphylococcus epidermidis* (CMCC(B)26069) and Gram-negative bacteria *Escherichia coli* (ATCC25922) were employed to evaluate the antibacterial properties of the rare oxide powders and coatings. The bacterial concentration of 10^6 CFU/ml was used in the sterilization and adhesion testing. The strains *Escherichia coli* and *Staphylococcus epidermidis* were subcultured in LB and TSB medium, respectively. The bacterial suspension was further seeded on specimen surfaces and cultured at 37 °C in a rocking incubator (Ref 20). The antibacterial performances were evaluated by the anti-adhesion properties and sterilization rates. For directly visualizing the bacterial adhesion behavior and accumulation morphologies, the bacteria were fixed using 2.5% glutaraldehyde for 24 h, dehydrated gradually in 10, 30, 50, 75, 100% alcohol and further dried at critical point at 25 °C. The obtained samples were coated with Au, then observed by SEM (S4800, Japan). The sterilization rates were analyzed by the spread plate method. The cytotoxicity of the Gd-doped HA coatings was measured by CCK-8 method. Human osteoblast-like cells (hFOB 1.19, National Centre for Cell Science (NCCS), Shanghai, China) were cultured in DME/F-12 1:1 medium with 10% FBS (Gibco, America), 2% double resistance (TransGen Biotech, Beijing) solution, in cell incubator with 37 °C and 5% CO_2 atmosphere. 3 × 10^4 cells/mL osteoblast were seeded on coatings.

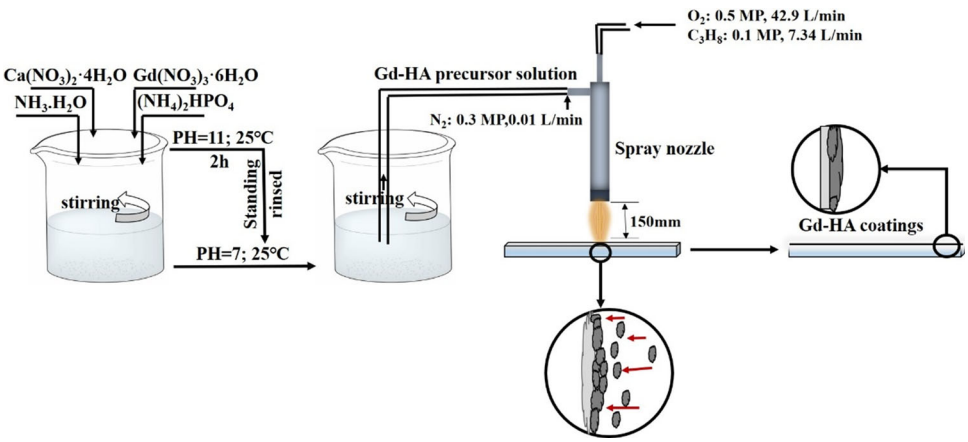

Fig. 1 Schematic depiction of the preparation process of Gd-HA slurry and subsequent coating

Results and Discussion

To gain a comprehensive understanding of the influence of rare earth elements on bacterial behaviors, the antibacterial effects of 14 rare earth elements (Eu, Gd, Ce, Nd, Y, La, Pr, Er, Sm, Ho, Tb, Yb, Lu, Dy) on both Gram-positive bacteria and Gram-negative bacteria were initially screened. After 12 h incubation, rare earth elements showed remarkable influence on growth viability of *E. coil* and *S. epidermidis* (Fig. 2). The antibacterial rate against *E. coil* is 67% for Eu, 42% for Gd, and 33% for Ce, respectively. Noticeably, rare earth elements show different effect on *S. epidermidis*. The antibacterial rate is 30% for Gd, 30% for Nd, and 25% for Er, respectively. Among 14 rare earth elements, the Gd could dramatically inhibit bacterial survival of both Gram-positive bacteria and Gram-negative bacteria.

Consequently, Gd^{3+} doped HA nano-crystallite with different Gd concentrations (5, 7.5 and 10 mol.% Gd incorporation) were synthesized by hydrothermal method to inhibit bacterial infection. The TEM image of the synthesized $Gd_{0.1}$-HA slurry shows an ultra-fine needle-like shape for the Gd^{3+} doped HA nanoparticles (Fig. 3a). In order to characterize the chemical composition distribution of Gd-HA, further EDX analysis of the Gd0.1-HA composite powders suggests the presence of Gd, Ca and P was detected (Fig. 3b, c and d). Additionally, the Gd elements are uniformly distributed in the composite powder (Fig. 3), suggesting that Gd^{3+} uniformly enters the HA lattice structure or ion-substituted HA during the synthesis process. The chemical composition, crystal size and lattice structural of biomimetic apatite could be regulated after incorporation of second phases (Ref 38, 39).

To further disclose the effects of Gd incorporation on shape, grain size and lattice structure of Gd-HA nanocrystalline, TEM, HRTEM and XRD were conducted. It is noted that, based on the TEM characterization, HA and Gd-HA nanoparticles present similar needle-like shape. However, the Gd-containing HA nanoparticles show finer grains (Fig. 4a-1 versus b-1). Mean grain size in the $Gd_{0.1}$-HA is ~ 100 nm in length and ~ 10 nm in diameter, while the Gd-free HA sample shows the grains of ~ 100 nm in length and ~ 30 nm in diameter. Recent studies already reported that high concentrations of rare earth Ce ions in HA resulted in reduction in crystallite size (Ref 40). In this study, it has been realized that during the synthesis of the Gd-HA nanocomposite powder, Gd inhibits HA grains nucleation and growth along diameter (Ref 24). The size of the $Gd^{3+}$of 0.0938 nm is close to that of Ca^{2+} of 0.1 nm. Surprisingly, the lattice spacing for Gd-HA slightly increased when Ca^{2+} ions are replaced by Gd^{3+} in the HA framework. The addition of Gd^{3+} ions interferes with the crystallization and increases vacancies and dislocations of nano-sized HA grains (Fig. 4a-2 versus b-2).

The chemical composition of 14 rare earth oxide powders was identified (Fig. 5a and b). Phase analysis of synthesized HA, Gd_x-HA (x = 0.05, 0.075, 0.1) powders and as-sprayed coatings was further characterized. Due to extremely low Gd^{3+} doping content, almost identical diffraction peaks are presented for HA and Gd-HA feedstocks. The sharp diffraction peaks were identified as the (002), (211), (300), (222) plane of HA located at 26.102°, 31.952°, 32.661°, 46.660°, respectively (Fig. 5c). Meanwhile, peak broadening attributed to the decreased grain size in the powders (Ref 41). The results of XRD were consistent with the results of TEM, both of which revealed the phenomenon of grain refinement after Gd incorporation in HA.

Figure 5(d) shows the XRD patterns of HA and Gd-HA coatings on Ti substrate. The diffraction peaks at 25.893°, 31.850°, 32.891°, 46.659° were identified as the (002), (211), (300), (222) planes of Gd-HA. Of special interest is peak location, which move slightly to the left in comparison with that of the pure HA powders, implying changed lattice distance of HA. As the increase doping of Gd^{3+}, the position of diffraction peaks move to smaller 2θ, namely, larger d-spacing values.

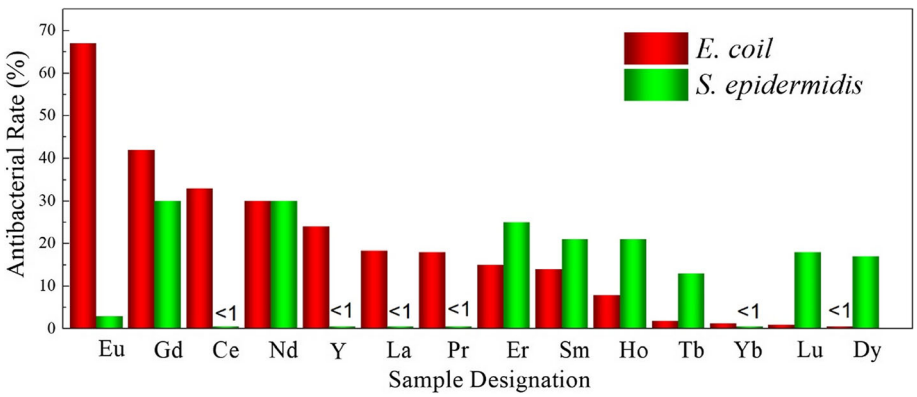

Fig. 2 Antibacterial rate of rare earth oxide for Gram-positive *E. coil* and Gram-negative *S. epidermidis*

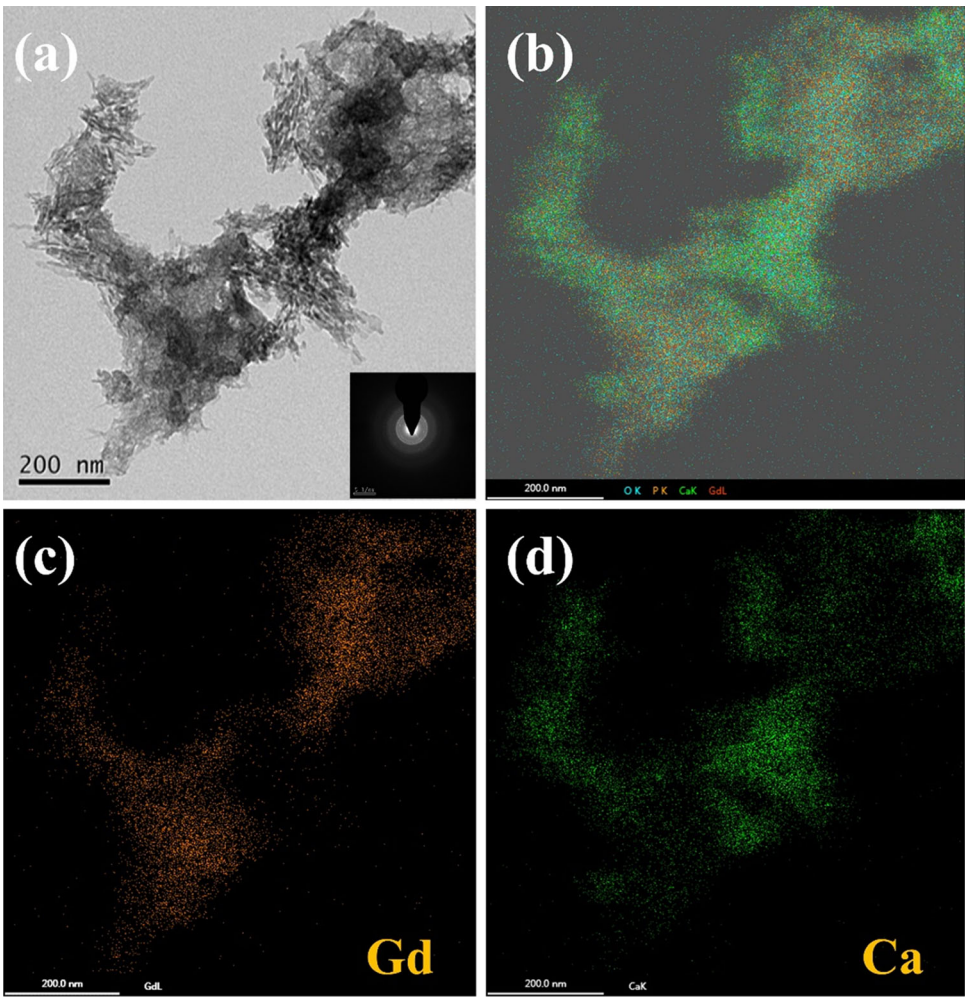

Fig. 3 TEM image and EDS mapping showing morphology (a) and element distribution of P (b), Gd (c) and Ca (d) of the Gd0.1-HA powder

Additionally, the diffraction peaks become narrower and sharper obviously after thermal spraying process. Some peaks display significant enhancement, especially at 40.728°, which indicated as the (311) crystal plane. This suggests possible recrystallization and grain growth of nanograins during thermal spraying process. Interestingly, with the increase of Gd content, the intensity of (311) plane gradually decreases. It can be attributed to Gd doping prevent the crystal growth along certain crystal plane. Furthermore, the high temperature process causes partial component decomposition and formation of DCPD ($CaHPO_4{\cdot}2H_2O$) and DCPA ($CaHPO_4$) in as-sprayed coatings (Ref 42). These peaks correspond to hydroxyapatite (JCDPS 9-432), DCPD (JCPDS 9-77), DCPA (JCPDS 9-80), $Gd(OH)_3$ (JCPDS 83-2037) and Gd_2O_3 (JCPDS 43-1014).

The HA, Gd0.05-HA, Gd0.075-HA, and Gd0.1-HA coatings were fabricated from synthesized HA slurry, 5 mol.% Gd-HA slurry, 7.5 mol.% Gd-HA slurry, and 10 mol.% Gd-HA slurry, respectively. Figure 6 presents the cross-section microstructure of as-sprayed coatings. The coatings are tightly bonded to the Ti substrates at their interfaces. The thickness of the coatings is less than 10 μm, which is enough to induce the biological response on the modified surface of the implant material. The porosity of the coatings is about 28-36% by image method. Surface morphology and roughness are key factors substantially influencing the interaction between cells and coating surfaces. The suspension flame sprayed coatings present broadened curves with slightly enhanced peak intensity, suggesting the retention of the initial nano-HA and nano-Gd-HA powders as well as well crystallinity of nanograins. Furthermore, the coatings deposited using Gd-free and Gd-based feedstocks show similar surface morphologies (Fig. 7a-1, b-1, c-1 and d-1). The nanosphere particles of 50 nm were retained in the as-sprayed coatings, illustrating recrystallization and crushing occurred during spraying process. Liquid flame spraying is a promising method for preparing nanostructured biological coatings (Ref 43).

Surface texture and roughness are critical parameters that physically affect bacterial sensing, attachment and adhesion on material surfaces. Recently, various

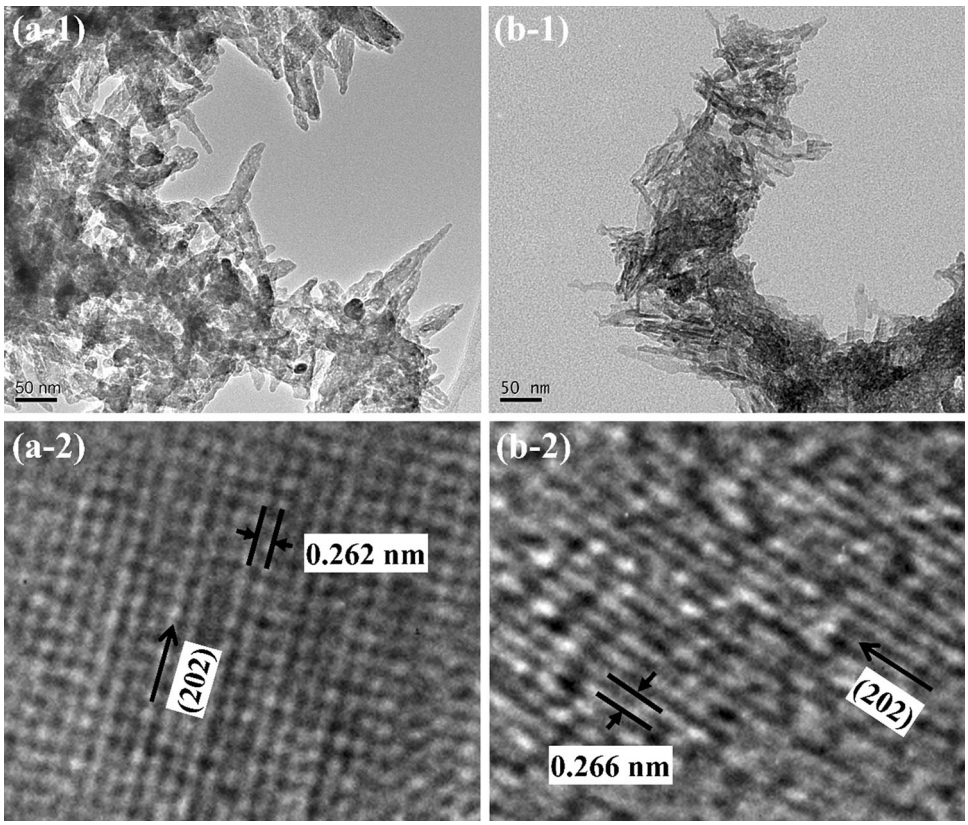

Fig. 4 TEM and HRTEM micrographs of the HA and Gd0.1-HA nanocrystalline. (a-1) TEM bright-field image shows needle-like HA nanograins, and (a-2) HRTEM image of (a-1) shows the lattice spacing of (202) plane of HA crystals. (b-1) TEM bright-field image shows ultra-fine needle-like Gd0.1-HA nanograins, and (b-2) HRTEM image of (b-1) reveals increased doping and vacancies of Gd0.1-HA crystals

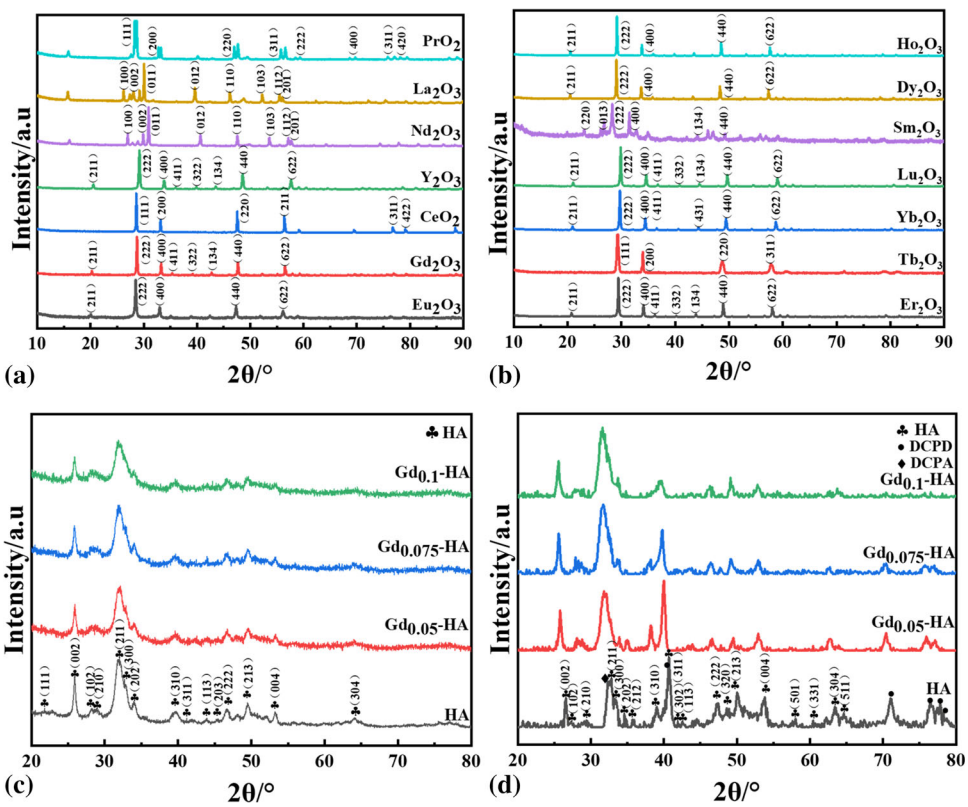

Fig. 5 XRD pattern curves of (a, b) original rare earth oxide powders, (c) synthesized HA and Gd-HA composite powders, and (d) as-sprayed HA and Gd-HA composite coatings

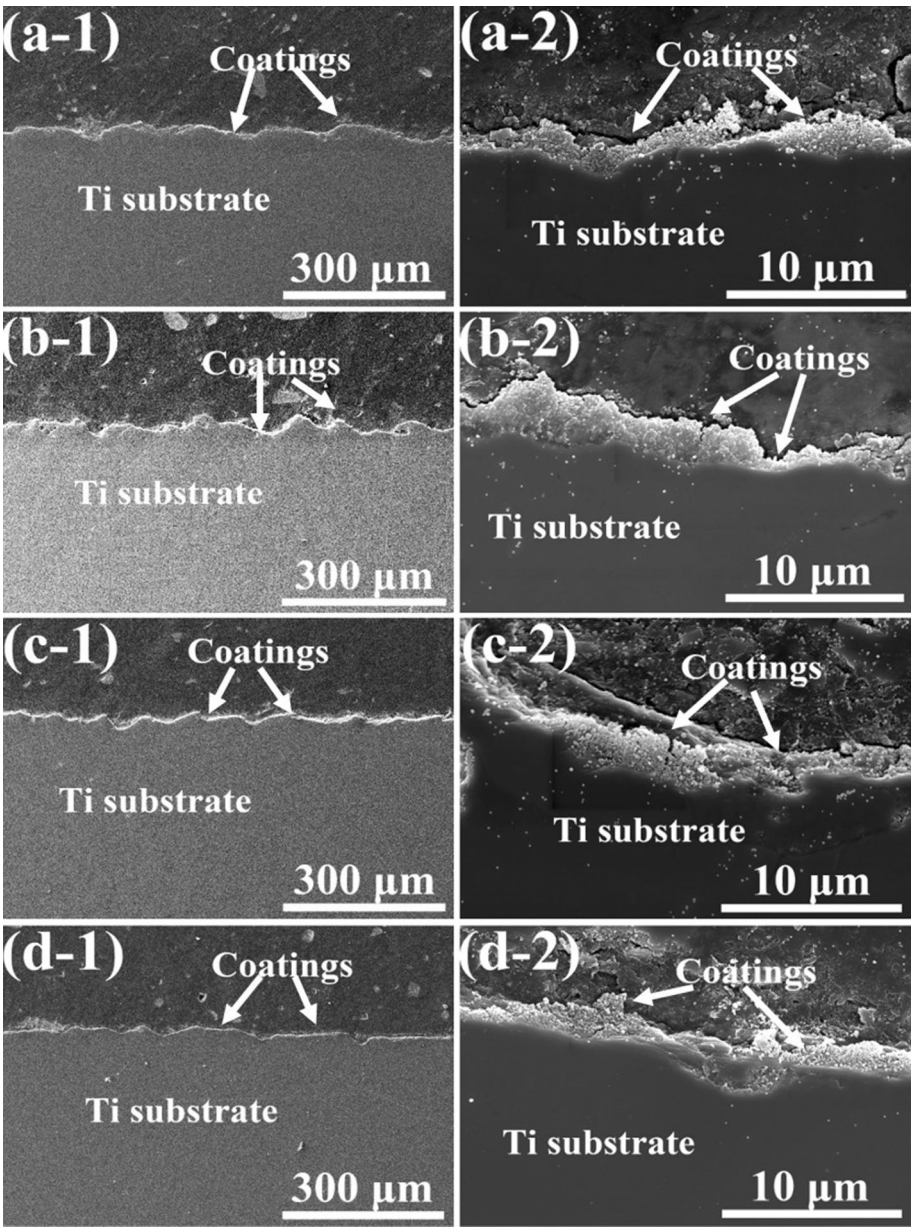

Fig. 6 Cross-section view of liquid flame sprayed coating: (a) HA coating, (b) Gd0.05-HA coating, (c) Gd0.075-HA coating and (d) Gd0.1-HA coating. 1. Low magnification, 2. High magnification

mechanisms involving relationship between surface roughness and bacterial adhesion have been proposed. Generally, most scholars revealed that adhesion forces increased with increasing surface roughness and greater cell adhesion to rougher surfaces by providing more anchor points for bacterial fimbriae (Ref 44). Nevertheless, others argued a contrary result that an increase of surface roughness did not influence or even inhibited the adhesion of bacteria. Average surface roughness (Ra) is the most frequently used parameters for characterizing surface topography (Ref 45). The topographical morphology was further examined by laser confocal microscope and disclosed roughness parameters as well as height distribution maps of the coating surfaces (Fig. 7a-2, b-2, c-2 and d-2). The roughness Ra show average values of approximately 4.5, 5, 10 and 6.5 μm for HA, $Gd_{0.05}$-HA, $Gd_{0.075}$-HA and $Gd_{0.1}$-HA coatings, respectively. Although rougher surfaces of thermal sprayed biological coatings usually facilitate bacterial adhesion, the antimicrobial effect of Gd element plays a more dominant role.

The antibacterial performances were evaluated by anti-adhesion and sterilization capacity of the coatings against Gram-negative *E. coil* and Gram-positive *S. epidermidis*. The interaction between the bacteria and coating were visualized by SEM through bacterial attachment. And, the viable microbial populations and antibacterial rate of suspended bacteria surrounding the coatings were estimated using the standard plate count (SPC) agar method (Ref 46).

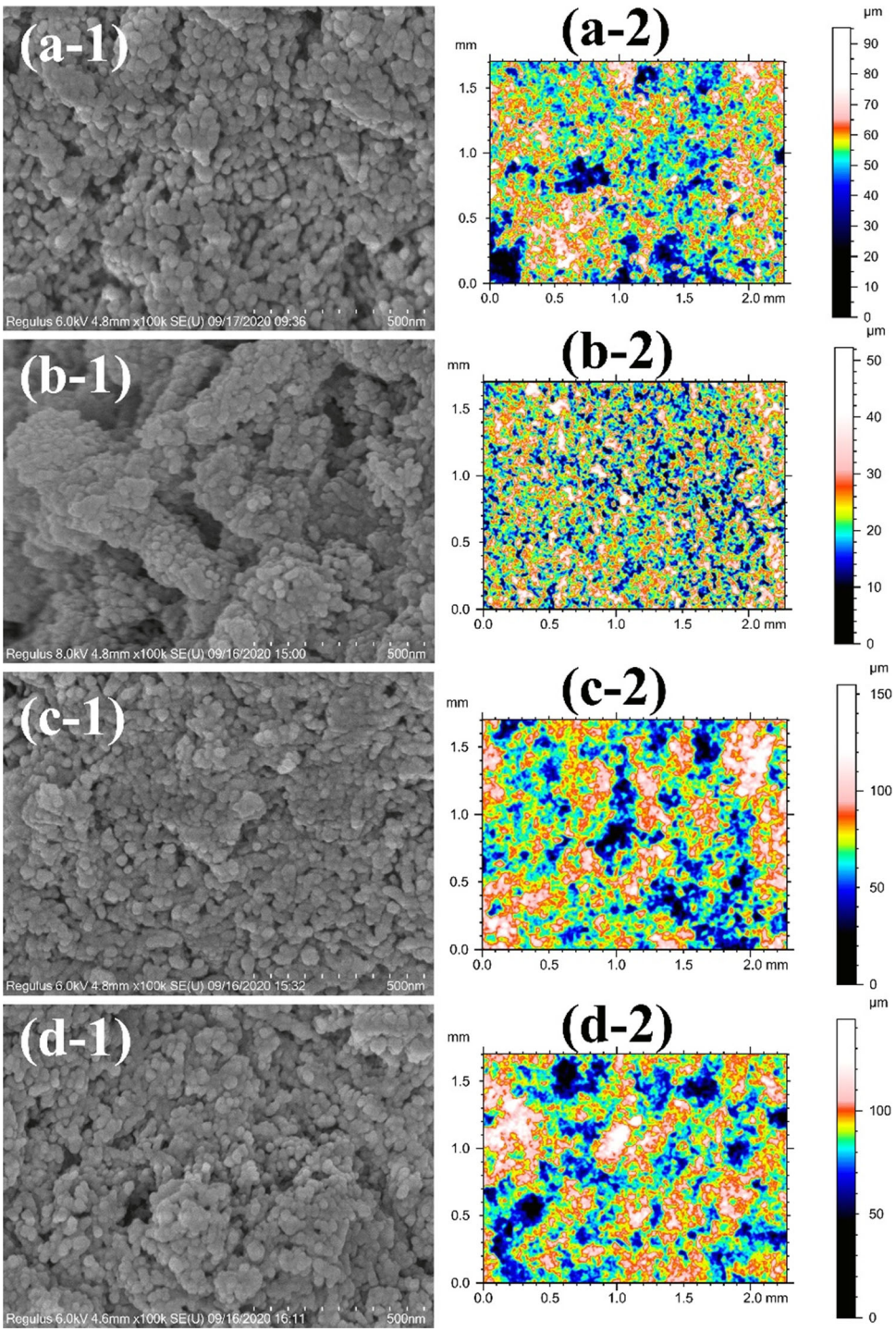

Fig. 7 Surface views of the (a) HA coating, (b) Gd0.05-HA coating, (c) Gd0.075-HA coating, and (d) Gd0.1-HA coating. 1. FESEM images, 2. Laser confocal microscope images

After being exposed in bacteria suspension for 4 h, *E. coli* and *S. epidermidis* bacteria already attached on the coating surfaces. The bacterial adhesion and colonization were realized underlying the partially biofilm formation (Fig. 8a-1 and a-2). Accordingly, the number of the adhered bacteria on HA and Gd-HA coating surfaces was counted by virtue of captured SEM images. More Gd in the coatings results in less recruited *E. coli.* The results show significantly prohibited attachment and survival of Gram-negative bacteria on the $Gd_{0.1}$-HA coating for 12 and 24 h as compared with that for 4 h (Fig. 8b-1 and c-1). In contrast, the $Gd_{0.1}$-HA coating slightly inhibited *S. epidermidis* bacterial adhesion (Fig. 8b-2 and c-2). Compared with Gram-positive bacteria, the Gd-HA coating tends to inhibit the adhesion of Gram-negative bacteria.

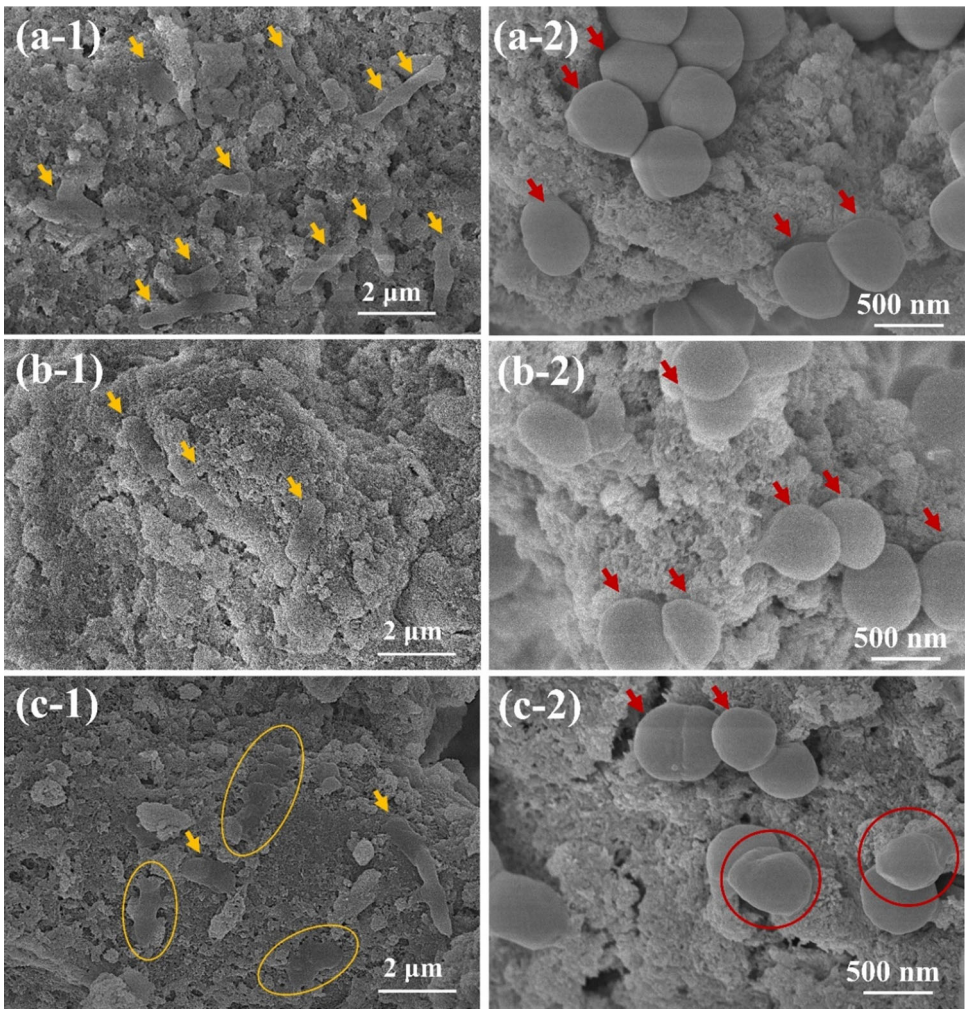

Fig. 8 SEM images of bacteria adhered on the Gd0.1-HA coatings after incubation for (a) 4 h, (b) 12 h and (c) 24 h. 1. *E. coli*, 2. *S. epidermidis*. (The yellow arrows highlight typical *E. coli* adhered on coating surface. The red arrows highlight typical *S. epidermidis* adhered on coating surface. The cell structure collapse of dead *E. coli* are marked by yellow circles, while the cell membrane shrinkage of dead *S. epidermidis* are enveloped by the red circles) (Color figure online)

In this case, it seems clear that contact of *E. coli* and *S. epidermidis* bacteria with the Gd-containing surface destroys the cellular structures of the bacteria by contact killing (Ref 47, 48) (Fig. 8c-1 and c-2). The dead bacteria are highlighted by the circles. The damage of cell wall of the bacteria and cell structure collapse could be the major regimes of the Gd^{3+}-induced bacteria-killing. Contact killing is an efficient way to inhibit the microbial survival and biofilm formation on the Gd-containing coatings.

To gain further insight into antifouling performances of the Gd-containing coatings, viability of planktonic bacteria surrounding the coatings in the bacterial suspension was used to test release-killing (Ref 49) properties of Gd^{3+} doped HA coatings. The white regions in agar plates were identified as the bacterial colonies. Through counting the colonies, the sterilization rates of the coatings for *E. coil* were calculated (Ref 45). After being incubated in bacteria solution for 4 h, the antibacterial rate is 3.8% for $Gd_{0.05}$-HA, 39.5% for $Gd_{0.75}$-HA, and 37.9% for $Gd_{0.1}$-HA. The antibacterial rate increases with the antibacterial time increasing. Further being cultured for 12 h, the antibacterial rate increases to 6.9% for $Gd_{0.05}$-HA, 52.1% for $Gd_{0.75}$-HA, and 64.4% for $Gd_{0.1}$-HA, indicating the more Gd doping, the more Gd^{3+} releasing at the same time and the higher antibacterial rate (Fig. 9a and b). This results in rare earth-based bactericidal coatings bearing both chemical-releasing bacteria-killing capacity and contact bacteria-killing capacity. However, after 24, 36 and 48 h of exposure, the antimicrobial activity of planktonic bacteria surrounding the coatings tends to be stable (Fig. 9a), suggesting that the Gd-HA coatings inhibit Gram-negative bacteria mainly by contact-killing or further enhanced Gd^{3+} concentration.

The $Gd_{0.1}$-HA coatings have no effect on significantly reduce the number of *S. epidermidis* bacterial attachments (Fig. 8). However, it is noted that excellent sterilization performances were further revealed for the Gd-containing coatings against *S. epidermidis.* After 4 h of exposure, the antibacterial rate are 10% for $Gd_{0.05}$-HA, 35.8% for $Gd_{0.75}$-HA, and 50% for $Gd_{0.1}$-HA. Interestingly, after 12 h exposure, ~ 100% *S. epidermidis* are already killed by the 10 mol.% Gd-HA coating (Fig. 10a). In contrast,

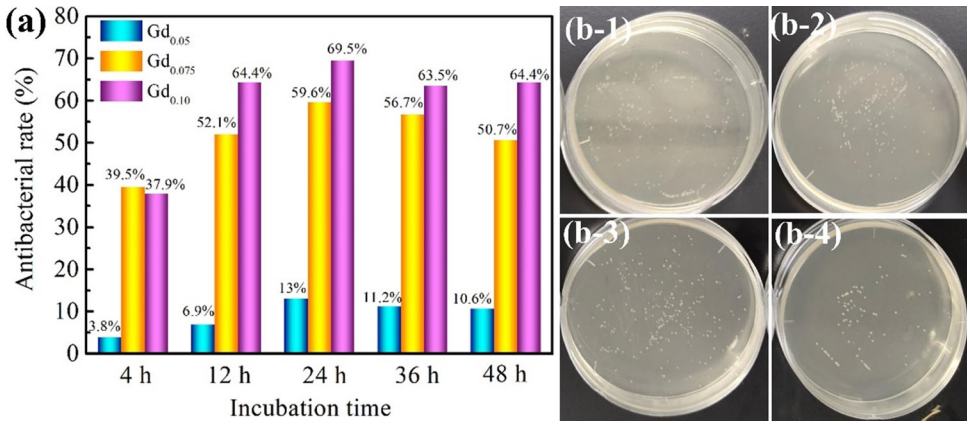

Fig. 9 (a) Examination of the sterilization rate of the Gd-HA coatings against bacteria *E. coli* and (b) the optical picture of the colony suspension diluted 10^3 times and cultivated on the agar plate for 12 h incubation. 1. Pure HA coating, 2. $Gd_{0.05}$-HA coating, 3. $Gd_{0.075}$-HA coating, 4: $Gd_{0.1}$-HA coating

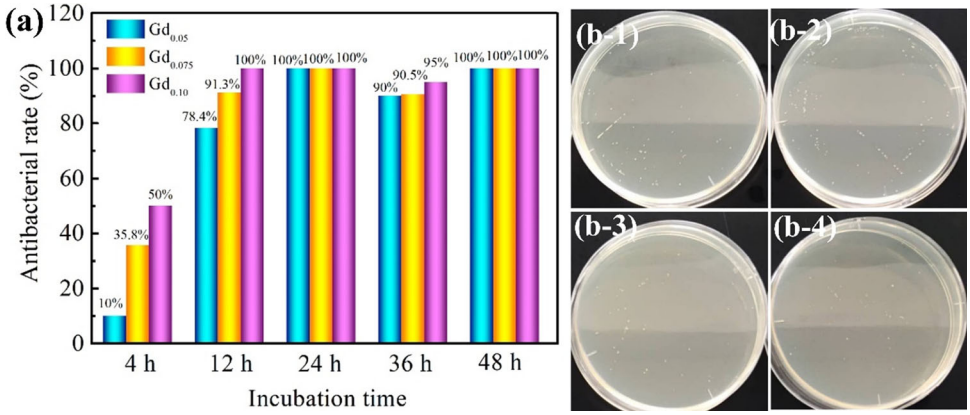

Fig. 10 (a) Examination of the sterilization rate of the Gd-HA coatings against bacteria *S. epidermidis*, and (b) the optical picture of the colony suspension diluted 10^3 times and cultivated on the agar plate for 12 h incubation. 1: pure HA coating, 2: $Gd_{0.05}$-HA coating, 3: $Gd_{0.075}$-HA coating, 4: $Gd_{0.1}$-HA coating

antibacterial rate of 10 mol.% Gd-HA coating against *E. coli* is 64.4% (Fig. 9a), indicating Gram-negative bacteria are more sensitive to Gd^{3+} ion invasion. For 12 h incubation, the higher the Gd dosage is the lower the number of *S. epidermidis* colonies proliferation and growth (Fig. 10b). Moreover, it is observed that the Gd-HA coatings have 90-100% extinguishing efficiency against Gram-positive bacteria *S. epidermidis* after being incubated in bacteria solution for 24, 36 and 48 h (Fig. 10a). The results show remarkably inhibited bacterial survival of *S. epidermidis* surrounding Gd-HA coatings which could be mainly attributed to Gd^{3+} release-killing. The HA as a degradable bioactive ceramic material can enhance the release and diffusion of Gd^{3+} ions into the surrounding environment. The accumulation of Gd^{3+} ion release increases gradually with the increase of degradation time. In view of the different cell structure and proliferation rate of Gram-negative bacteria and Gram-positive bacteria, Gd^{3+} ions are more likely to attack the cell walls of Gram-positive bacteria and thus exhibit higher antimicrobial efficiency.

Biocompatibility of element Gd is still controversial. The toxicity of Gd^{3+} depends on its concentration. In this study, osteoblast cells (hFOB 1.19) were used for cytotoxicity evaluation of Gd-containing coatings. The effects of the Gd-doped HA coatings on cell proliferation

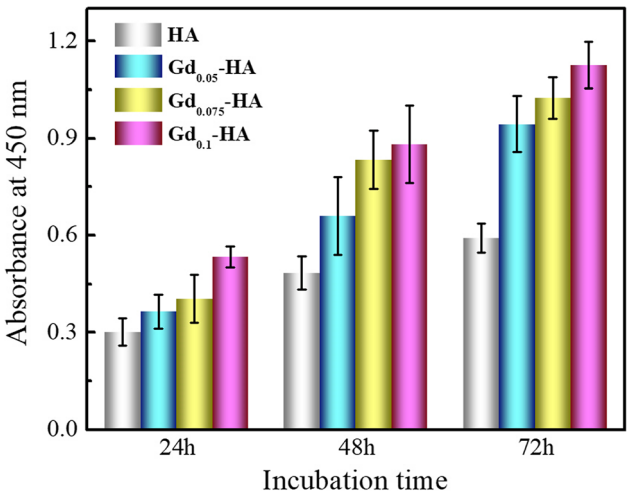

Fig. 11 Osteoblast viability assay at 24, 48 and 72 h by CCK8 analysis

performances were measured by CCK-8 method using pure HA coating as control. Compared with HA coating, Gd_x-HA (x = 0.05, 0.075, 0.1) coatings exhibited no cytotoxicity and even promoted bone cell proliferation with the incubation time of 24, 48 and 72 h (Fig. 11). Consequently, liquid flame sprayed Gd-HA coatings exhibited great

potential to be used as antibacterial materials with appropriate Gd content.

Conclusions

Nanostructured Gd-HA composite coatings were successfully deposited on titanium alloy by liquid flame spraying. The original nanostructure of the feedstock was obviously retained in the HA and Gd-HA coatings. The incorporation of Gd showed excellent cytocompatibility and promoted osteoblasts proliferation. The Gd-containing bioactive ceramic coatings performed both chemical-releasing bacteria-killing capacity and contact bacteria-killing capacity. Gd-HA coatings significantly inhibited Gram-negative bacteria *E. coli* adhesion and survival mainly by contact-killing. The *S. epidermidis* surrounding Gd-HA coatings were rapidly killed by Gd^{3+} ions release. The development of the novel rare earth-based composite coatings by the thermal spray approach could provide more opportunities for promotion of medical devices with excellent antibacterial infection properties on condition that Gd dosage should be carefully controlled.

Acknowledgments This research was supported by National Natural Science Foundation of China (Grant # 52071329), Zhejiang Provincial Natural Science Foundation of China (Grant # LY18C100003), The Youth Innovation Promotion Association of the Chinese Academy of Sciences, China (Grant # 2020299) and S&T Innovation 2025 Major Special Programme of Ningbo, China (Grants # 2020Z095). Jiangxi Province Key Research and Development Projects of China (Grants # 20192BBE50033 and 20202BBEL53031).

References

1. M. Niinomi, Y. Liu, M. Nakai, H.H. Liu, and H. Li, Biomedical Titanium Alloys with Young's Moduli Close to that of Cortical Bone, *Regen. Biomater.*, 2016, **3**, p 173-185
2. K. Marycz, A. Smieszek, S. Targonska, S.A. Walsh, K. Szustakiewicz, and R.J. Wiglusz, Three Dimensional (3D) Printed Polylactic Acid with Nano-hydroxyapatite Doped with Europium(III) Ions (nHAp/PLLA@Eu($^{3+}$)) Composite for Osteochondral Defect Regeneration and Theranostics, *Mater. Sci. Eng. Mater.*, 2020, **110**, p 110634. https://doi.org/10.1016/j.msec.2020.110634
3. Y.K. Kim, S.G. Kim, J.H. Byeon, H.J. Lee, I.U. Um, S.C. Lim, and S.Y. Kim, Development of a Novel Bone Grafting Material Using Autogenous Teeth, *J. Oral Maxil Surg.*, 2010, **109**(4), p 496-504
4. L. Sun, C.C. Berndt, K.A. Gross, and A. Kucuk, Material Fundamentals and Clinical Performance of Plasma-Sprayed Hydroxyapatite Coatings: A Review, *J. Biomed. Mater. Res.*, 2001, **10**(58), p 570-593
5. C.L. Popa, A. Groza, P. Chapon, C.S. Ciobanu, R.V. Ghita, R. Trusca, M. Ganciu, and D. Predoi, Physicochemical Analysis of the Polydimethylsiloxane Interlayer Influence on a Hydroxyapatite Doped with Silver Coating, *J. Nanomaters*, 2015, **2015**, p 1-10
6. K. Ohta, M. Kikuchi, J. Tanaka, and H. Eda, Synthesis of c Axes Oriented Hydroxyapatite Aggregate, *Chem. Lett.*, 2002, **2**(4), p 36-38
7. Y. Liu, W. Hou, R. Lupoi, S. Yin, J. Huang, and H. Li, Microscopic Visualization of Cell – Cold Sprayed Bio-coating Interfaces: An Intermediate Layer Formed During the Culturing Mediates the Behaviors of the Cells, *Appl. Surf. Sci.*, 2020, **529**, p 1-9
8. P. Baskaran, A. Udduttula, and V. Uthirapathy, Development and Characterisation of Novel Ce-Doped Hydroxyapatite-Fe_3O_4 Nanocomposites and Their In Vitro Biological Evaluations for Biomedical Applications, *IET Nanobiotechnol.*, 2018, **12**(2), p 138-146
9. H. Hu, K. Johani, A. Almatroudi, K. Vickery, B. Van Natta, M.E. Kadin, G. Brody, M. Clemens, C.Y. Cheah, S. Lade, P.A. Joshi, H.M. Prince, and A.K. Deva, Bacterial Biofilm Infection Detected in Breast Implant-Associated Anaplastic Large-Cell Lymphoma, *Plast. Reconstr. Surg.*, 2016, **137**(6), p 1659-1669
10. K. Szyszka, J. Rewak-Soroczynska, A. Dorotkiewicz-Jach, K.A. Ledwa, A. Piecuch, M. Giersig, Z. Drulis-Kawa, and R.J. Wiglusz, Structural Modification of Nanohydroxyapatite $Ca_{10}(PO_4)_6(OH)_2$ Related to Eu($^{3+}$) and Sr($^{2+}$) Ions Doping and Its Spectroscopic and Antimicrobial Properties, *J. Inorg. Biochem.*, 2020, **203**, p 110884
11. A. Fihri, C. Len, R.S. Varma, and A. Solhy, Hydroxyapatite: A Review of Syntheses, Structure and Applications in Heterogeneous Catalysis, *Coord. Chem. Rev.*, 2017, **347**, p 48-76
12. M. Yetmez, Z.E. Erkmen, C. Kalkandelen, A. Ficai, and F.N. Oktar, Sintering Effects of Mullite-Doping on Mechanical Properties of Bovine Hydroxyapatite, *Mate. Sci. Eng.*, 2017, **77**, p 470-475
13. Y. Li, C.P. Ooi, C.H. Ning, and K. Aik-Khor, Synthesis and Characterization of Neodymium(III) and Gadolinium(III)-Substituted Hydroxyapatite as Biomaterials, *Int. J. Appl. Cera*, 2009, **6**(4), p 501-512
14. Ž. Radovanović, B. Jokić, D. Veljović, S. Dimitrijević, V. Kojić, R. Petrović, and D. Janaćković, Antimicrobial Activity and Biocompatibility of Ag^+ and Cu^{2+} Doped Biphasic Hydroxyapatite/α-Tricalcium Phosphate Obtained from Hydrothermally Synthesized Ag^+ and Cu^{2+} Doped Hydroxyapatite, *Appl. Surf. Sci.*, 2014, **307**, p 513-519
15. S. Eto, H. Miyamoto, T. Shobuike, I. Noda, T. Akiyama, M. Tsukamoto, M. Ueno, S. Someya, S. Kawano, M. Sonohata, and M. Mawatari, Silver Oxide-Containing Hydroxyapatite Coating Supports Osteoblast Function and Enhances Implant Anchorage Strength in Rat Femur, *J. Orthop. Res.*, 2015, **33**(9), p 1391-1397
16. T. Wakabayashi, A. Ymamoto, A. Kazaana, Y. Nakano, Y. Nojiri, and M. Kashiwazaki, Antibacterial, Antifungal and Nematicidal Activities of Rare Earth Ions, *Biol. Trace Elem. Res.*, 2016, **174**(2), p 464-470
17. A. Jordens, Y.P. Cheng, and K.E. Waters, A Review of the Beneficiation of Rare Earth Element Bearing Minerals, *Miner. Eng.*, 2013, **41**, p 97-114
18. S. Zaichick, V. Zaichick, V. Karandashev, and S. Nosenko, Accumulation of Rare Earth Elements in Human Bone within the Lifespan, *Metallomics*, 2011, **3**(2), p 186-194
19. G. Pagano, M. Guida, F. Tommasi, and R. Oral, Health Effects and Toxicity Mechanisms of Rare Earth Elements-Knowledge Gaps and Research Prospects, *Ecotoxicol. Environ. Saf.*, 2015, **115**, p 40-48
20. K. Saranya, S. Bhuvaneswari, S. Chatterjee, and N. Rajendran, Biocompatible Gadolinium-Coated Magnesium Alloy for Biomedical Applications, *J. Mater. Sci.*, 2020, **55**(25), p 11582-11596

21. Y. Lin, Z. Yang, and J. Cheng, Preparation, Characterization and Antibacterial Property of Cerium Substituted Hydroxyapatite Nanoparticles, *J. Rare Earth*, 2007, **25**(4), p 452-456
22. K.H. Thompson and C. Orvig, Editorial: Lanthanide Compounds for Therapeutic and Diagnostic Applications, *Chem. Soc. Rev.*, 2006, **35**(6), p 499-505
23. M.E. Bartolini, J. Pekar, D.R. Chettle, F. McNeill, A. Scott, J. Sykes, F.S. Prato, and G.R. Moran, An Investigation of the Toxicity of Gadolinium Based MRI, Contrast Agents Using Neutron Activation Analysis, *Mag. Reson. Imaging*, 2003, **21**(5), p 541-544
24. M.F. Cipreste, A.M. Peres, A.A.C. Cotta, F.H. Aragón, A.D.M. Antunes, A.S. Leal, W.A.A. Macedo, and E.M.B. de Sousa, Synthesis and Characterization of 159 Gd-Doped Hydroxyapatite Nanorods for Bioapplications as Theranostic Systems, *Mater. Chem. Phys.*, 2016, **181**, p 301-311
25. C. Huang, Y. Huang, N. Tian, Y. Tong, and R. Yin, Preparation and Characterization of Gelatin/Cerium(III) Film, *J. Rare Earth*, 2010, **28**(5), p 756-759
26. D. Bian, J. Deng, N. Li, X. Chu, Y. Liu, W. Li, H. Cai, P. Xiu, Y. Zhang, Z. Guan, Y. Zheng, Y. Kou, B. Jiang, and R. Chen, In Vitro and In Vivo Studies on Biomedical Magnesium Low-Alloying with Elements Gadolinium and Zinc for Orthopaedic Implant Applications, *ACS Appl. Mater. Interfaces.*, 2018, **10**, p 4394-4408
27. F. Liao, X.Y. Peng, F. Yang, Q.F. Ke, Z.H. Zhu, and Y.P. Guo, Gadolinium-Doped Mesoporous Calcium Silicate/Chitosan Scaffolds Enhanced Bone Regeneration Ability, *Mater. Sci. Eng., C*, 2019, **104**, p 109999
28. D. Csontos, U. Zülicke, P. Brusheim, and H.Q. Xu, Lande-Like Formula for the g Factors of Hole-Nanowire Subband Edges, *Phys. Rev. B*, 2008, **78**(3), p 1-4
29. Y. Huang, J. He, L. Gan, X. Liu, Y. Wu, F. Wu, and Z.-W. Gu, Osteoconductivity and Osteoinductivity of Porous Hydroxyapatite Coatings Deposited by Liquid Precursor Plasma Spraying: In Vivo Biological Response Study, *Biomed. Mater.*, 2014, **9**(6), p 065007-065018
30. P. Bansal, G.T. Singh, and H.S. Sidhu, Investigation of Corrosion Behavior and Surface Properties of Plasma Sprayed HA/Sr Reinforced Coatings on CoCr Alloys, *Mater. Chem. Phys.*, 2020, **253**, p 123330
31. R. Gonzalez, H. Ashrafizadeh, A. Lopera, P. Mertiny, and A. McDonald, A Review of Thermal Spray Metallization of Polymer-Based Structures, *J. Therm. Spray Technol.*, 2016, **6**(7), p 415-438
32. M. Gell, E.H. Jordan, M. Teicholz, B.M. Cetegen, N.P. Padture, L. Xie, D. Chen, X. Ma, and J. Roth, Thermal Barrier Coatings Made by the Solution Precursor Plasma Spray Process, *J. Therm. Spray Technol.*, 2007, **17**(1), p 124-135
33. E. Gozali, S. Kamnis, and S. Gu, Analysis of Liquid Feedstock Behavior in High Velocity Suspension Flame Spraying for the Development of Nanostructured Coatings, *J. Therm. Spray Technol.*, 2013, **13**(15), p 418-425
34. G. Bolelli, V. Cannillo, R. Gadow, A. Killinger, L. Lusvarghi, J. Rauch, and M. Romagnoli, Effect of the Suspension Composition on the Microstructural Properties of High Velocity Suspension Flame Sprayed (HVSFS) Al_2O_3 Coatings, *Surf. Coat. Technol.*, 2010, **204**(8), p 1163-1179
35. E. Bemporad, G. Bolelli, V. Cannillo, D. De Felicis, R. Gadow, A. Killinger, L. Lusvarghi, J. Rauch, and M. Sebastiani, Structural Characterisation of High Velocity Suspension Flame Sprayed (HVSFS) TiO_2 Coatings, *Surf. Coat. Technol.*, 2010, **204**(23), p 3902-3910
36. C.H. Hou, S.M. Hou, Y.S. Hsueh, J. Lin, H.C. Wu, and F.H. Lin, The In Vivo Performance of Biomagnetic Hydroxyapatite Nanoparticles in Cancer Hyperthermia Therapy, *Biomaterials*, 2009, **30**(23–24), p 3956-3960
37. J.L. Ong and D.C.N. Chan, Hydroxapatite and Its Use as a Coating in Dental Implants: A Review, *Crit. Rev. Biomed. Eng.*, 2017, **45**(1–6), p 291-320
38. Z.Y. Li, W.M. Lam, C. Yang, B. Xu, G.X. Ni, S.A. Abbah, K.M. Cheung, K.D. Luk, and W.W. Lu, Chemical Composition, Crystal Size and Lattice Structural Changes After Incorporation of Strontium into Biomimetic Apatite, *Biomaterials*, 2007, **28**(7), p 1452-1460
39. F. Heshmatpour, S.H. Lashteneshaee, and M. Samadipour, Study of In Vitro Bioactivity of Nano Hydroxyapatite Composites Doped by Various Cations, *J Inorg Organomet*, 2018, **28**(5), p 2063-2068
40. V. Sanysl and R. Raja, Structural and Antibacterial Activity of Hydroxyapatite and Fluorohydroxyapatite Co-substituted with Zirconium-Cerium Ions, *Appl. Phys A*, 2016, **122**(132), p 1-12
41. W.P. Wijesinghe, M.M. Mantilaka, E.V. Premalal, H.M. Herath, S. Mahalingam, M. Edirisinghe, R.P. Rajapakse, and R.M. Rajapakse, Facile Synthesis of Both Needle-Like and Spherical Hydroxyapatite Nanoparticles: Effect of Synthetic Temperature and Calcination on Morphology, Crystallite Size and Crystallinity, *Mater. Sci. Eng. C Mater. Biol. Appl.*, 2014, **42**, p 83-90
42. S. Jarudilokkul, W. Tanthapanichakoon, and V. Boonamnuayvittaya, Synthesis of Hydroxyapatite Nanoparticles Using an Emulsion Liquid Membrane System, *Colloid Surface A*, 2007, **296**(1–3), p 149-153
43. Y. Huang, L. Song, T. Huang, X. Liu, Y. Xiao, Y. Wu, F. Wu, and Z. Gu, Characterization and Formation Mechanism of Nano-Structured Hydroxyapatite Coatings Deposited by the Liquid Precursor Plasma Spraying Process, *Biomed. Mater.*, 2010, **5**(5), p 054113-054420
44. N. George, M. Mahon, and A. McDonald, Bactericidal Performance of Flame-Sprayed Nanostructured Titania-Copper Composite Coatings, *J. Therm. Spray Technol.*, 2010, **19**(5), p 1042-1053
45. S. Sharma, Y.A. Jaimes-Lizcano, R.B. McLay, P.C. Cirino, and J.C. Conrad, Subnanometric Roughness Affects the Deposition and Mobile Adhesion of Escherichia Coli on Silanized Glass Surfaces, *Langmuir*, 2016, **32**(21), p 5422-5433
46. X. Li, M. Qi, C. Li, B. Dong, J. Wang, M.D. Weir, S. Imazato, L. Du, C.D. Lynch, L. Xu, Y. Zhou, L. Wang, and H.H.K. Xu, Novel Nanoparticles of Cerium-Doped Zeolitic Imidazolate Frameworks with Dual Benefits of Antibacterial and Anti-Inflammatory Functions Against Periodontitis, *J. Mater. Chem. B*, 2019, **7**(44), p 6955-6971
47. H. Ruan, C. Fan, X. Zheng, Y. Zhang, and Y. Chen, In Vitro Antibacterial and Osteogenic Properties of Plasma Sprayed Silver-Containing Hydroxyapatite Coating, *Sci. Bull.*, 2009, **54**(23), p 4438-4445
48. M.C. Dodd, H.E. Kolher, and A.V. Gunten, Oxidation of Antibacterial Compounds by Ozone and Hydroxyl Radical: Elimination of Biological Activity During Aqueous Ozonation Processes, *Environ. Sci. Technol.*, 2009, **43**, p 2498-2504
49. P. Liu, Y. Liu, Z.X. Xie, A.X. Hou, P. Shen, and S.S. Qu, Microcalorimetric Studies of the Action of Er^{3+} on Halobacterium Halobium R1 Growth, *Bio Trace Elem. Res.*, 2005, **104**, p 275-285